ACS APPLIED MATERIALS & INTERFACES

Research Article

www.acsami.org

Structure, MC3T3-E1 Cell Response, and Osseointegration of Macroporous Titanium Implants Covered by a Bioactive Microarc Oxidation Coating with Microporous Structure

Rui Zhou,[†] Daqing Wei,*[,†] Su Cheng,[‡] Wei Feng,[†] Qing Du,[†] Haoyue Yang,[†] Baoqiang Li,[†] Yaming Wang,[†] Dechang Jia,[†] and Yu Zhou[†]

[†]Department of Materials Science and Engineering, Harbin Institute of Technology, Harbin 150001, People's Republic of China

[‡]Department of Mechanical Engineering, School of Architecture and Civil Engineering, Harbin University of Science and Technology, Harbin 150001, People's Republic of China

Supporting Information

ABSTRACT: Macroporous Ti with macropores of 50−400 μm size is prepared by sintering Ti microbeads with different diameters of 100, 200, 400, and 600 μm. Bioactive microarc oxidation (MAO) coatings with micropores of 2−5 μm size are prepared on the macroporous Ti. The MAO coatings are composed of a few TiO_2 nanocrystals and lots of amorphous phases with Si, Ca, Ti, Na, and O elements. Compared to compact Ti, the MC3T3-E1 cell attachment is prolonged on macroporous Ti without and with MAO coatings; however, the cell proliferation number increases. These results are contributed to the effects of the space structure of macroporous Ti and the surface chemical feature and element dissolution of the MAO coatings during the cell culture. Macroporous Ti both without and with MAO coatings does not cause any adverse effects in vivo. The new bone grows well into the macropores and micropores of macroporous Ti with MAO coatings, showing good mechanical properties in vivo compared to Ti, MAO-treated Ti, and macroporous Ti because of its excellent osseointegration. Moreover, the MAO coatings not only show a high interface bonding strength with new bones but also connect well with macroporous Ti. Furthermore, the pushing out force for macroporous Ti with MAO coatings increases significantly with increasing microbead diameter.

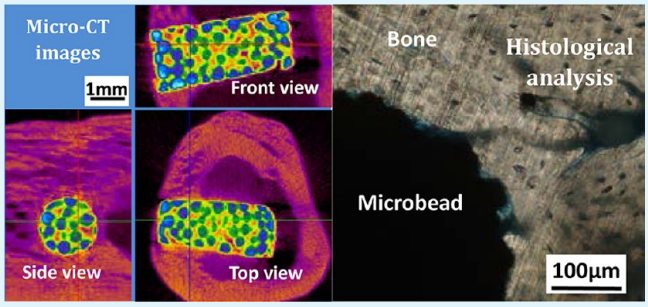

KEYWORDS: *macroporous Ti, MC3T3-E1 osteoblast, microarc oxidation, osseointegration, mechanical properties*

1. INTRODUCTION

Porous implants such as Ti and its alloys have been noticed extensively in the biomaterial regions.[1−3] As is well-known, the macropores of 50−300 μm size of the porous implants determine the bone ingrowth and control the mechanical properties for successful implantation.[4−8] First, it is well believed that suitable initial implant stabilization and an acceptable porous geometry to allow uninhibited bone ingrowth are useful for successful bone ingrowth.[1−3] After implantation, the implants with macropores could provide three-dimensional mechanical interlocking between the bone and implant for secure implant fixation.[1−3] Second, Ti and its alloys show much higher Young's moduli, which could result in a "stress-shielding" phenomenon.[9] In order to control Young's modulus, bending, and yield strengths for biomedical applications, macroporous Ti has been used in the previous research.[9]

A number of approaches to fabricate three-dimensional macroporous Ti have been reported, including sintering of Ti powders[9] or wires.[10] These methods could produce porous materials with high porosity and well-interconnected structure, but the porosity and pore size of materials are difficult to control. Compared to the above methods, vacuum sintering of Ti microbeads to fabricate macroporous Ti with macropores has some advantages, such that the macropore size and mechanical properties of macroporous Ti can be controlled by adjusting the Ti microbead diameter.[9]

The effect of the micropore of 2−5 μm size on the cell attachment is not very clear. At the same time, the fabrication technique for the uniform micropore is not extensive. However, a microarc oxidation (MAO) technique is suitable for preparing the uniform micropore. At the same time, the MAO method is a relatively convenient and effective technique to deposit bioactive ceramic coatings on the surfaces of Ti and its alloys with strong interface bonding,[11] which has received much attention in recent years.[11−21]

As reported, the pore sizes of many macroporous Ti and its alloy implants are at one scale of macropore.[9] The implants with a double-scale porous structure have been less reported. Thus, a hybrid technique of vacuum sintering of Ti microbeads

Received: December 10, 2013
Accepted: March 3, 2014
Published: March 3, 2014

   dx.doi.org/10.1021/am405680d | ACS Appl. Mater. Interfaces 2014, 6, 4797−4811

and MAO is used to prepare the double-scale porous structure in recent research.[22−24] At the same time, the MAO technique is usually used to modify samples with a flat surface.[11−21] The formation of bioactive coatings with good mechanical properties on macroporous Ti is very difficult according to the previous investigation.[5,22−24] However, the application of the MAO technique on macroporous Ti can resolve this problem well. The formation of the MAO coatings on macroporous Ti is discussed in recent research.[23] Moreover, the MAO coatings on macroporous Ti have a good apatite formation ability in a simulated body fluid.[24] However, the effects of the double-scale porous structure on the cell attachment, proliferation, and osseointegration are not reported. This work reports the transmission electron microscopy (TEM) microstructures of the MAO coatings on macroporous Ti, the effects of the macroporous structure and MAO coatings on the MC3T3-E1 osteoblast response, and the formation of bones in macroporous Ti with MAO coatings. At the same time, the mechanical properties of the interface bonding between the implants and new bones are investigated in this work.

2. EXPERIMENTAL PROCEDURES

2.1. Sample Preparation. Four kinds of commercial Ti microbeads with mean diameters of 100, 200, 400, and 600 μm supplied by Baoji Haibao Special Metal Materials Co., Ltd., of China were sintered to fabricate macroporous Ti. During the preparation for macroporous Ti, Ti microbeads were also filled in graphite molds of 10 × 10 × 10 mm^3 size for machining implants and in molds of 10 × 10 × 3 mm^3 size for the cell test. Boron nitride lubricant was sprayed on the inner wall of the molds to avoid the reaction between graphite and Ti microbeads during sintering. At last, these molds with Ti microbeads were sintered under a vacuum environment (1 × 10^{-3} Pa) without applied pressure by holding at a temperature of 1450 °C for 2 h with a heating rate of 10 °C/min. After sintering, the cubic macroporous Ti samples (10 × 10 × 10 mm^3) were machined to cylindrical samples (⌀ 2 × 6 mm^3) for MAO. For an in vitro experiment, Ti plates (10 × 10 × 1 mm^3) as the control were ground with 400#, 800#, and 1000# abrasive papers, washed with acetone and distilled water, and dried at 40 °C.

Ti plates (10 × 10 × 1 mm^3) and macroporous Ti (⌀ 2 × 6 mm^3 and 10 × 10 × 3 mm^3) were used as anodes, and stainless steel plates were used as cathodes in an electrolytic bath. An electrolyte was prepared by the dissolution of reagent-grade chemicals of $Ca(CH_3COO)_2{\cdot}H_2O$ (6.3 g/L), Na_2SiO_3 (13.2 g/L), EDTA-2Na (15 g/L), and NaOH (15 g/L) into deionized water. The applied voltage of 500 V was used to prepare MAO coatings on the Ti plates and macroporous Ti. The frequency, duty cycle, and oxidizing time were 600 Hz, 8.0%, and 5 min, respectively. The temperature of the electrolyte was kept at 40 °C by a cooling system. The samples were divided into four groups including Ti, pTi, Ti-MAO, and pTiMAO, and the corresponding treatment parameters are shown in Table 1.

2.2. Structure Characterization. *2.2.1. Scanning Electron Microscopy (SEM) and Energy-Dispersive X-ray Spectrometry (EDS).* SEM (Helios Nanolab 600i, FEI Co., Hillsboro, OR) was used to observe the surface morphologies. In addition, the elemental concentrations of the sample surface were detected by EDS (EDAX Inc., Mahwah, NJ) with the SEM system.

2.2.2. TEM and Focus Ion Beam (FIB). TEM (Tecnai G2F30, FEI Co., Hillsboro, OR) with an accelerated voltage of 300 kV was used to observe the microstructure of the pTiMAO400 coating. In the TEM operation, the morphology of the pTiMAO400 coating was observed. Selected-area electron diffraction (SAED), microzone electron diffraction (MZED), and high-resolution of TEM (HRTEM) were acquired to analyze the TiO_2 nanocrystals and amorphous phase. FIB (Helios Nanolab 600i, FEI Co., Hillsboro, OR) was used to prepare the TEM sample.

2.3. MC3T3-E1 Cell Response. *2.3.1. MC3T3-E1 Cell Adhesion Test.* MC3T3-E1 osteoblasts of rat (ShangHai Institutes for Biological Sciences, Chinese Academy of Sciences) were used for the cell test in this work. The samples were placed in a 24-well culture plate, and the MC3T3-E1 cells with a cell density of 5 × 10^5 mL^{-1} were seeded on the samples. Then, the 24-well culture plate was added by α-modified Eagle's medium (α-MEM) with penicillin and 10% fetal bovine serum (FBS). After the 24-well culture plate was stored in a humidified incubator with 5% CO_2 at 37 °C for 0.5, 1, 2, and 4 h, the culture was terminated. The samples were taken out and carefully washed with phosphate-buffered saline (PBS) three times to remove the MC3T3-E1 cells that did not adhere to the samples. These samples were transferred into a new 24-well culture plate containing 0.3 mL of pancreatic enzyme. After the pancreatic enzyme digested for 3 min, α-MEM was added to terminate the pancreatic enzyme digest. At last, the cell suspension was obtained for detecting the numbers of adhered cells. The cell adhesion ratio of Ln was calculated by eq 1:

$$Ln = (Tn/Jn) \times (Sp/Ss) \times 100\% \quad (1)$$

where Tn is the number of the adhered cells, Jn is the number of the seeded cells, Sp is the area of the bottom of the 24-well culture plate, and Ss is the area of the surface of the sample.

2.3.2. MC3T3-E1 Cell Proliferation Test. The Ti, pTi, Ti-MAO, and pTiMAO groups were placed in a 24-well culture plate. The MC3T3-E1 cells after pancreatic enzyme digest with a cell density of 5 × 10^4 mL^{-1} were seeded on the samples of the Ti, pTi, Ti-MAO, and pTiMAO groups. After culturing for 1, 4, 7, and 10 days, the samples were washed with PBS three times. Then, the washed samples were cultured in α-MEM with the addition of penicillin and 10% FBS, 200 μL of media, and 20 μL of a cell counting kit-8 (CCK-8) solution in a humidified incubator with 5% CO_2 at 37 °C for 4 h. Then the 100 μL cultured solution was taken out to a 96-well culture plate. A microplate reader for enzyme-linked immunosorbent assay (ELISA) was used to detect the OD value of optical absorbance at a wavelength of 450 nm. The cell proliferation ratio of OD_a was calculated by eq 2:

$$OD_a = (OD_s - OD_b)/(OD_c - OD_b) \times 100\% \quad (2)$$

where OD_s originated from the culture plate containing media with cells, CCK-8, and the samples, OD_c originated from the culture plate containing media with cells and CCK-8, and OD_b originated from blank controls.

2.3.3. Activity of the Alkaline Phosphatase (ALP) Test. The Ti, pTi, Ti-MAO, and pTiMAO groups were placed in a 24-well culture plate, and the MC3T3-E1 cells with a cell density of 1 × 10^5 mL^{-1} were seeded on the samples. After culturing for 3 days, the culture solution was removed and samples were carefully washed with PBS three times. The 24-well culture plate was added with 200 μL of Triton

Table 1. Sample Labels and Corresponding Treatment Parameters

group	sample label	material	microbead diameter (μm)	MAO treatment (yes/no)
Ti	Ti	Ti		no
pTi	pTi100	porous Ti	100	no
	pTi200	porous Ti	200	no
	pTi400	porous Ti	400	no
	pTi600	porous Ti	600	no
Ti-MAO	Ti-MAO	Ti		yes
pTiMAO	pTiMAO100	porous Ti	100	yes
	pTiMAO200	porous Ti	200	yes
	pTiMAO400	porous Ti	400	yes
	pTiMAO600	porous Ti	600	yes

X-100 and kept at 4 °C overnight. The analyzed solution was produced by uniformly mixing 30 μL of Triton X-100 after treatment of the MC3T3-E1 cells and 100 mL of ALP (Alkaline Phosphatase Activity Assay Kit, Jc-A0059). The microplate reader for ELISA was used to detect the value of optical absorbance at a wavelength of 520 nm. The bicinchoninic acid (BCA) method was used to measure the concentration of proteins in the 24-well culture plate. The activity of ALP was calculated by eq 3:

$$H_{OD} = (C_{OD} - K_{OD})/(B_{OD} - K_{OD})Z_{BCA}/D_{BCA} \quad (3)$$

where H_{OD} is the activity of ALP, C_{OD} is the value of optical absorbance of the culture plate with ALP and Triton X-100 after treatment of the cell, K_{OD} is the value of optical absorbance of the culture plate with ALP, B_{OD} is the value of optical absorbance of the 24-well culture plate, Z_{BCA} is the standard concentration of phenol, and D_{BCA} is the concentration of proteins in the 24-well culture plate.

2.3.4. SEM Observation of the Cells. The samples after the MC3T3-E1 cell culture were fixed in pH = 7.2 PBS containing 2.5% glutaraldehyde for 1.5 h at 4 °C. Then the fixed samples were washed with pH = 7.2 PBS three times in intervals of 10 min. After washing, the samples were fixed with 1% osmium tetroxide for 1 h. After treatment in osmium tetroxide, the samples were washed with pH = 7.2 PBS three times in intervals of 10 min. After washing, the samples were dehydrated with alcohol with concentrations of 50%, 70%, and 90% in intervals of 10 min and then dehydrated with 100% alcohol three times in intervals of 10 min. The dehydrated samples were treated in a mixed solution of 100% alcohol and tertiary butanol with a ratio of 1:1 for 15 min and treated in pure tertiary butanol for 15 min. After these treatments, the samples were further frozen at −20 °C for 30 min and dried in a freeze-drying machine for 4 h. At last, the samples were coated with a thin gold film for SEM observation.

2.3.5. Microfilament Observation by Confocal Laser Scanning Microscopy (CLSM). The sterilized Ti, pTi, Ti-MAO, and pTiMAO groups were placed in a 24-well culture plate, and the MC3T3-E1 cells with a cell density of 5×10^4 mL^{-1} were seeded on the samples. After seeding of the cells, the samples were cultured in a humidified incubator with 5% CO_2 at 37 °C for 4 h. When the culture was terminated, the samples were transferred in a new 24-well culture plate and then washed with PBS three times. The washed samples were immersed in a 4% paraformaldehyde solution for 10 min and stored in a refrigerator at 4 °C overnight. The treated samples were further washed with PBS three times and treated with 0.1% triton for 30 min. After this treatment, the samples were washed with PBS three times and colored with rhodamine B at room temperature in a dark place. Further, the colored samples were washed with PBS three times and sealed with glycerol for observation by CLSM.

2.3.6. Statistical Analysis. The software of *SAS6.0* was used to perform statistical analysis by one-way analysis of variance, and the data have a statistical difference when $p < 0.05$. In the cell attachment and proliferation number tests, each group with at least eight samples was measured. In addition, three samples in each group after cell attachment were observed by SEM and CLSM. In the test of the change in the elemental concentration of the MAO coatings during the cell culture, each group with at least five samples was used and measurement was carried out with at least three independent repeats.

2.4. Implantation, Osseointegration Analysis, and Biomechanical Property Investigation. *2.4.1. Implantation in the Tibia of Rabbits.* The Ti, pTi, Ti-MAO, and pTiMAO groups were performed on 24 healthy and mature New Zealand rabbits with weights of 2.5−3 kg, with half of them being male. The rabbits were chosen randomly to be observed at three periods of 4, 8, and 12 weeks after implantation. The New Zealand rabbits were fixed on an operation table, and a 40 mg/kg pentobarbital sodium solution was injected into the ear vein of the rabbits. The fur near the center of the rabbit legs was sheared, and the skin was sterilized with 2% lodophor and 75% alcohol. After injection of 2% lidocaine, the skin, fascia, and periosteum were sliced in sequence, and then the surface of the tibia was exposed. Teeth plant equipment was used to machine a hole of ⌀ 2×6 mm^3 under a cooling condition by saline water. After removal of the bone chippings, the samples were implanted into the holes, and then the muscular fascia, subcutaneous tissue, and skin were sutured in sequence. After implantation, each rabbit was injected with an antibiotic of gentamicin in a dose of 1 mL/day for 3 days. The normal dietary intake of the rabbit performed well, and the sutured line was removed after implantation for 10 days.

2.4.2. Taking Out the Implants. After implantation for 4, 8, and 12 weeks, the rabbits were put to death by injection of air into the ear vein of the rabbits. Immediately, the tibia was detached from the rabbits for further investigation, and the remaining organs were treated safely.

2.4.3. Radiographic Evaluation. X-ray images of the implants were taken by an X-ray digital photographic technique (XPLORER1600; IDC Co., Toronto, Ontario, Canada) with an alternating-current power of 380 V.

2.4.4. Measurement of the Pushing-Out Force. The universal testing machine (Instron-1186; Instron Co., Norwood, MA) was used to measure the pushing-out force between the implant and tibia. A workpiece holder with a penetrator of 2 mm diameter was used to fix the sample.

2.4.5. SEM Observation. The pushed-out samples from the tibia were immersed in 2.5% glutaraldehyde overnight. Then the samples were washed with PBS three times for 15 min and fixed with tannin for 1 h. The fixed samples were then washed with PBS and dehydrated with alcohol with different concentrations of 50%, 70%, 90%, and 100% and acetone in sequence. The dehydrated samples were further dried and coated with a thin gold film for SEM observation.

2.4.6. Micro-CT Test. The taken-out tibias with implants were scanned by micro-CT (SKYSCAN1076; Skyscan Co., Brussels, Belgium) with a scanning rate of 6°/min and a resolution of 9 μm to detect the growth of new bone and analyze the interface structure between the implants and bones. The data and images were analyzed by *CT-ANY* software, which was equipped on the micro-CT machine. The setting of the colors also referred to the previous research.[4]

2.4.7. Embedding and Tissue Sectioning. (1) Dehydration: The taken-out tibias with implants were immersed in a 10% formaldehyde solution for 1 week. Then, the samples were dehydrated with alcohol with different concentrations of 70% (for 12 h), 90% (for 12 h), 95% (for 30 h), and 100% (for 24 h) and a mixed solution of 100% alcohol and 100% ether with a ratio of 1:1 (for 12 h), chloroform (for 36 h), and xylene (for 12 h).

(2) Immersion: A total of 500−750 mL of methyl methacrylate was put into a separatory funnel with the addition of 250 mL of 5% NaOH. After uniform mixing, the solution in the bottom layer was drained away. This operation was repeated three times, then distilled water was used instead of NaOH, and the same operations were also repeated three times. After this operation, the solution was dehydrated by the addition twice of anhydrous calcium chloride with a ratio of 1000 mL:500 g. Then, solution was filtered, and the filtrates were collected and stored at 4 °C. On the second day, the modified methyl methacrylate solution was checked, and if there were ice crystals, it was dehydrated again. Then, three kinds of immersion solutions (I−III) were further produced. Immersion solution I was produced by mixing 75 mL of a modified methyl methacrylate solution and 25 mL of dibutyl phthalate for 3 h in a magnetic stirrer. Immersion solution II was produced by mixing 75 mL of a modified methyl methacrylate solution, 25 mL of dibutyl phthalate, and 1 g of benzoyl peroxide for 4 h in a magnetic stirrer. Immersion solution III was produced by mixing 75 mL of a modified methyl methacrylate solution, 25 mL of dibutyl phthalate, and 2.5 g of benzoyl peroxide for 6 h in a magnetic stirrer. The samples were immersed in immersion solutions I−III in sequence for 2 days at 4 °C.

(3) Polymerization treatment and tissue sectioning: The immersed samples were put into a 10 mL tube, and fresh immersion solution III was added to the tube. Then the tube was capped, and two needles were inserted for release of the gas resulting from polymerization. After setting overnight, the tube containing the samples was put into a vacuum vessel for creation of a vacuum in the tube. Then the tube containing the samples was polymerized in a water bath at 37−39 °C for 48 h, until the embedded samples were formed. The embedded

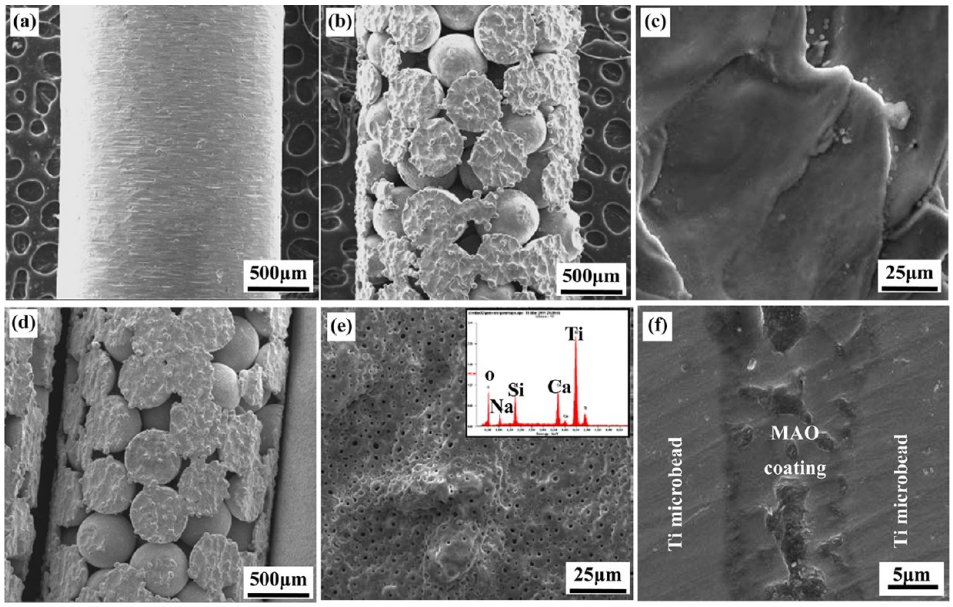

Figure 1. Surface and interior morphology and EDS spectrum of the Ti, pTi400, and pTiMAO400 implants: (a) Ti; (b) macroporous structure of pTi400; (c) high magnification of part b; (d) macroporous structure of pTiMAO400; (b) high magnification of part d and EDS result of the MAO coating; (f) interior morphology of the pTiMAO400 implant.

samples were sliced along the axial of the implants into flakes with thicknesses of 100 μm by a sawing slicing machine (Leica 1600).

2.4.8. Histological Analysis. Solution A was produced by mixing 1 g of toluidine blue and 10 mL of 70% alcohol. The colored solution was prepared by mixing solution A and 9 mL of a 1%NaOH solution and filtering the mixed solution. The slicings were washed with distilled water for 20 min and immersed in the colored solution for 2 h. Then the colored samples were washed with a 70% alcohol solution, and at last the washed samples were observed by a microscope.

3. RESULTS

3.1. SEM Morphology and EDS Analysis. Figure 1 shows the surface and interior morphologies as well as EDS results of the Ti, pTi400, and pTiMAO400 implants. Parts a and b of Figure 1 show the typical surface morphologies of Ti and pTi400 implants; the macropore size of pTi400 is about 300 μm. Figure 1c is an enlarged image of Figure 1b. The typical macroporous structure of the pTiMAO400 implant is shown in Figure1d, and this macroporous structure is similar to that of pTi400, indicating that the MAO treatment has no obvious effect on the macroporous structure of pTi. The whole surface of the pTiMAO400 implant is covered by the MAO coating, as shown in Figure 1e, which is a magnified micrograph for the surface morphology of Figure 1d. Apparently, the MAO coating exhibits many typical micropores with sizes of 2−5 μm, different from the surface of pTi under high-magnification observation (Figure 1c). The EDS result shows that the main chemical composition of the MAO coating is Ti, Ca, Si, Na, and O elements. Of course, the MAO technique does not break off the macroporous structure of pTi. Figure 1f shows the cross-sectional SEM morphology of the interior of the pTiMAO400 implant. The MAO coating with a thickness of 2−5 μm is on the surfaces of two Ti microbeads, which are connected together by the MAO coating. In addition, the other pTiMAO implants also show good formation of the MAO coatings on the surface and interior of the pTiMAO implants (not shown here).

3.2. TEM Analysis. The recent study[23] indicates that the microbead diameter has an effect on the surface morphology and elemental concentration such as Ca, Si, and Na of the pTiMAO samples. However, the phase compositions of the four kinds of pTiMAO samples are similar according to XRD,[23] containing an amorphous phase and TiO_2. Thus, the TEM micrographs of pTiMAO400 are shown in the current paper.

Figure 2 shows the TEM micrographs and SAED, MZED, and HRTEM patterns of the pTiMAO400 implant. The whole morphology of the TEM sample prepared by FIB is shown in Figure 2a. Two typical regions are observed including regions A and A*, as shown in Figure 2a. Region A contains some nanocrystals, while region A* does not show any change in the diffraction contrast by rotation of the TEM sample during the observation process, suggesting an amorphous phase. Figure 2b is the magnified micrograph of region A in Figure 2a. Region B shows a typical amorphous phase according to its diffraction pattern, as shown in Figure 2c. Sure, no crystal is observed according to the HRTEM pattern, as shown in Figure 2d. Figure 2e shows the MZED pattern from the crystal of region C in Figure 4b; this crystal is anatase according to pattern indexing. Region D shows diffraction rings for nanocrystals as well as weak diffraction for the amorphous phase, as shown in Figure 2f. The further observation of the HRTEM pattern reveals a coexisting region of the amorphous phase and TiO_2 nanocrystals at region D, as shown in Figure 2g. The EDS results indicate that the main elemental compositions of the amorphous region are Si, Ca, Ti, and O elements (not shown here). TEM results indicate that the main phase composition of the MAO coating is the amorphous phase and few TiO_2 nanocrystals are embedded in the amorphous phase.

3.3. MC3T3-E1 Cell Response. *3.3.1. Cell Adhesion Observation by SEM.* Figure 3 shows the typical SEM images of the MC3T3-E1 cells adhering to the pTiMAO group for 4 h. The many MC3T3-E1 cells appear at the connection region between Ti microbeads when the microbead diameter is small such as pTiMAO100, as shown by white arrows in Figure 3a. A similar phenomenon is observed on the other samples such as pTiMAO600, as shown in Figure 3b. However, the cells are also found at the other places of the microbeads, such as Figure

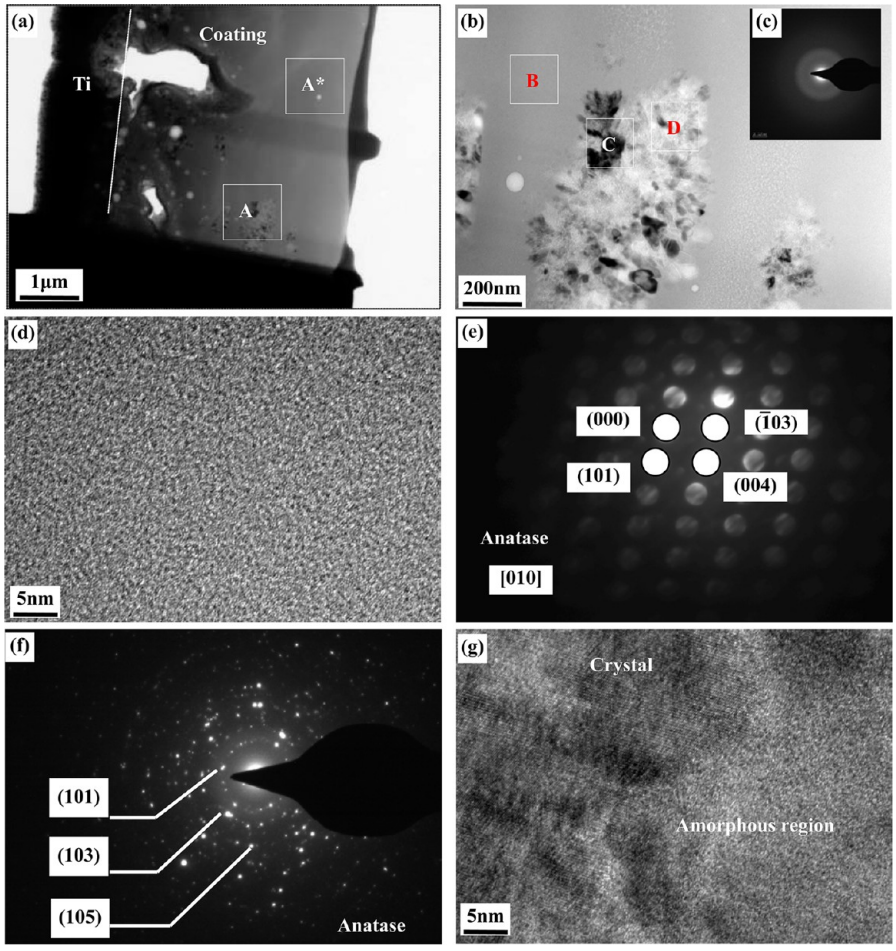

Figure 2. TEM micrographs and SAED, MZED, and HRTEM patterns of the pTiMAO400 coating: (a) TEM micrograph of the whole sample prepared by FIB; (b) TEM micrograph of region A shown in part a; (c) amorphous phase diffraction pattern of region B shown in part b; (d) HRTEM pattern of region B shown in part b; (e) MZED pattern of the TiO_2 crystal shown by region C in part b; (f) SAED pattern of region D shown in part b; (g) HRTEM pattern of region D shown in part b. Note: region A contains lots of crystals, and region A* only contains the amorphous phase; region B consists of the amorphous phase; region C mainly consists of crystals; region D is composed of nanocrystals and the amorphous phase.

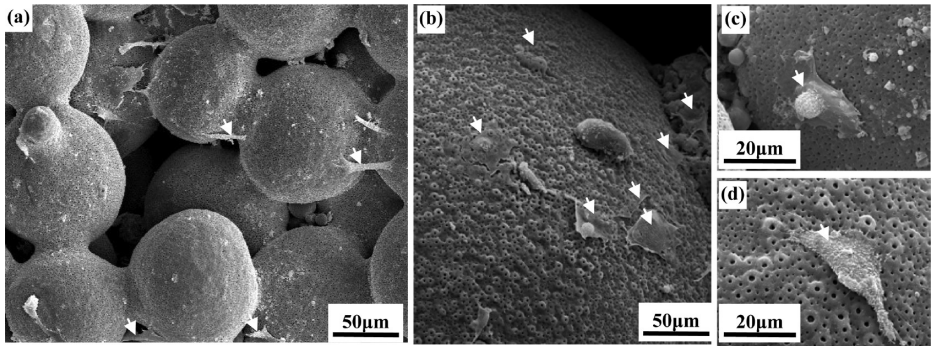

Figure 3. SEM images of the MC3T3-E1 cells adhering to the pTiMAO group for 4 h: (a) pTiMAO100; (b) pTiMAO600; (c) high magnification of pTiMAO100; (d) high magnification of pTiMAO600. Note: the cells are marked by white arrows.

3b,d. At high magnification, analysis by SEM reveals that the pTiMAO group causes a well spread of MC3T3-E1 cells by 4 h of the culture, as shown in Figure 3c,d, on which cells appear to be highly flat. A similar phenomenon is observed on the surface of the pTi group compared to the pTiMAO group (not shown here), and the SEM images for cell attachment on Ti and Ti-MAO are reported in recent research.[25]

3.3.2. Cell Adhesion Observation by CLSM. Figure 4 shows CLSM images of the MC3T3-E1 cells on Ti, Ti-MAO, pTi400, and pTiMAO400 after cell culturing for 4 h, which further demonstrates clearly the adhering status of the MC3T3-E1 cells. It can be seen that the MC3T3-E1 cells distribute randomly on Ti and Ti-MAO. In pTi400 and pTiMAO400, they appear at the connection regions between two Ti microbeads and at the locations around the connection regions

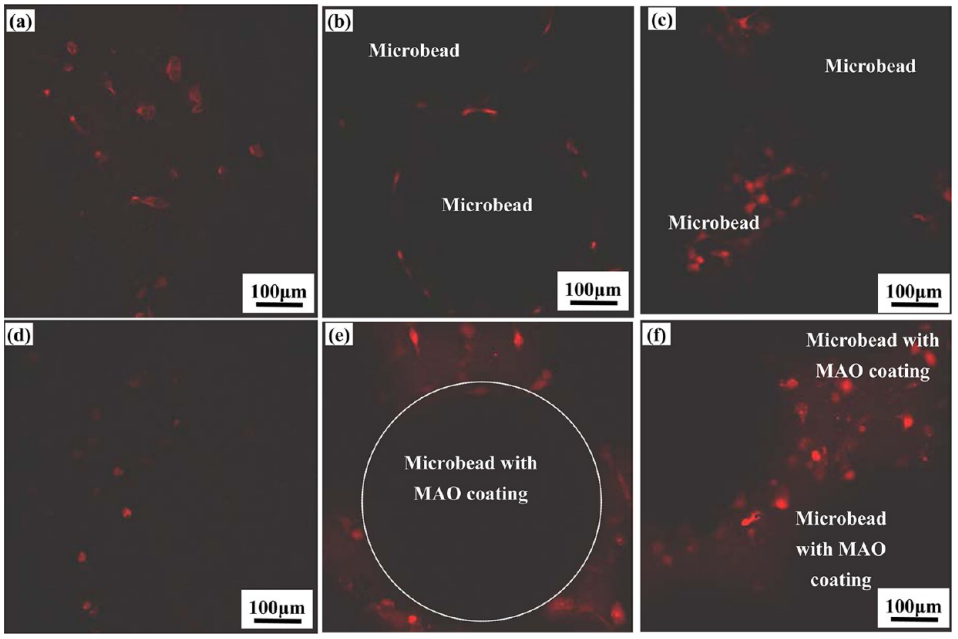

Figure 4. CLSM images of the MC3T3-E1 cells cultured for 4 h on Ti, Ti-MAO, pTi400, and pTiMAO400: (a) Ti; (b) cells at the connection region by microbeads of pTi400; (c) cells around the connection region and the top of the microbeads of pTi400; (d) Ti-MAO; (e) cells at the connection regions by microbeads of pTiMAO400; (f) cells around the connection region and the top of the microbeads of pTiMAO400.

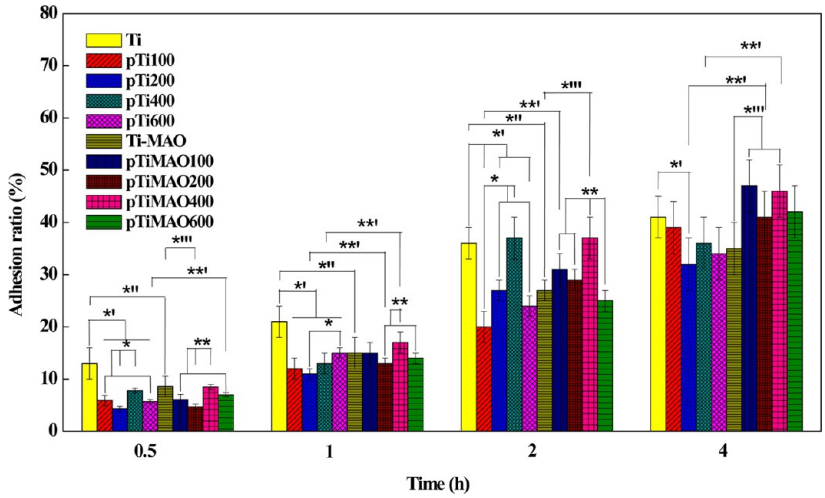

Figure 5. The adhesion ratio of the MC3T3-E1 cells on the surfaces of the four groups (Ti, Ti-MAO, pTi, and pTiMAO). Note: * means the comparison among the samples in the pTi group; ** means the comparison among the samples in the pTiMAO group; *′ means the comparison between Ti and the samples in the pTi group; *″ means the comparison between Ti and Ti-MAO; *‴ means the comparison between Ti-MAO and the samples in the pTiMAO group; **′ means the comparison between the samples of the pTi group and the samples in the pTiMAO group. *, **, *′,*″,*‴, and **′ represent $p < 0.05$. The software of *SAS6.0* was used to perform statistical analysis, and the sample number of each material is more than 8.

and the top of the microbeads of pTi400 and pTiMAO400, as shown in Figure 4b,c,e,f, similar to the SEM observation results. In addition, similar results are observed on the surfaces of pTi compared to pTiMAO (not shown here).

3.3.3. Cell Adhesion Ratio. Figure 5 shows the adhesion ratio of the MC3T3-E1 cells on the surfaces of the four groups (Ti, pTi, Ti-MAO, and pTiMAO).

(1) In Ti & pTi groups: A higher cell adhesion ratio is observed on Ti than on all of the samples in the pTi group after culturing for 0.5 and 1 h ($p < 0.05$). After culturing for 2 h, the cell adhesion ratio on Ti is similar to that on pTi400 and still higher than that on the other samples in the pTi group ($p < 0.05$). After culturing for 4 h, the cell adhesion ratio on Ti is only higher than that on pTi200 and, however, similar to that on the other samples in the pTi group. These results indicate that the cell adhesion ratio on the pTi group decrease compared to that of Ti. At the same time, the difference in the cell adhesion ratio between Ti and pTi reduces with increasing culturing time from 0.5 to 4 h.

(2) In Ti & Ti-MAO groups: Compared to Ti, a lower cell adhesion ratio is observed on the surface of Ti-MAO after culturing for 0.5, 1, and 2 h. However, no significant difference in the cell adhesion ratio between Ti and Ti-MAO is found after culturing for 4 h. These results indicate that formation of the MAO coating on Ti prongs the cell adhesion.

dx.doi.org/10.1021/am405680d | *ACS Appl. Mater. Interfaces* 2014, 6, 4797−4811

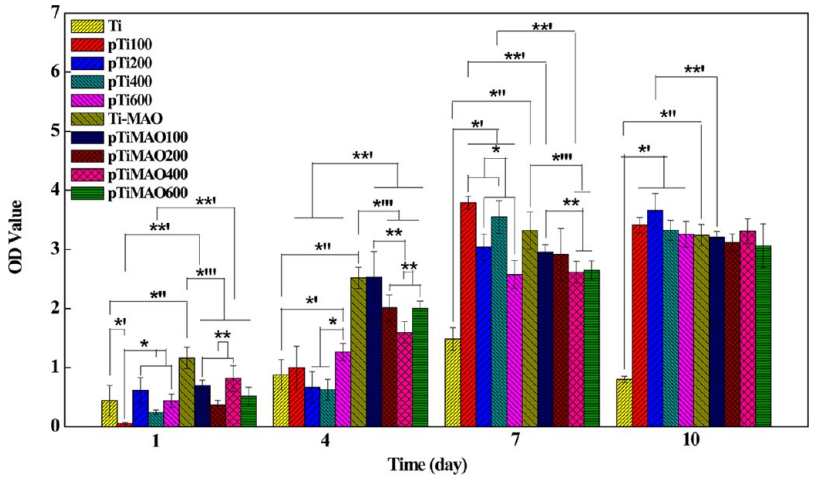

Figure 6. Proliferation number of the MC3T3-E1 cells on the surfaces of the four groups (Ti, Ti-MAO, pTi, and pTiMAO). Note: * means the comparison among the samples in the pTi group; ** means the comparison among the samples in the pTiMAO group; *′ means the comparison with Ti and the samples in the pTi group; *″ means the comparison with Ti and Ti-MAO; *‴ means the comparison with Ti-MAO and the samples in the pTiMAO group; **′ means the comparison with the samples in the pTi group and the samples in the pTiMAO group. *, **, *′,*″,*‴, and **′ represent $p < 0.05$. The software of *SAS6.0* was used to perform statistical analysis, and the sample number of each material is more than 8.

(3) In pTi & pTiMAO groups: The difference in the cell adhesion ratio appears after culturing for 0.5−4 h, such as pTi600 & pTiMAO600 at 0.5 h ($p < 0.05$), pTi400 & pTiMAO400 and pTi200 & pTiMAO200 at 1 h ($p < 0.05$), pTi100 & pTiMAO100 at 2 h ($p < 0.05$), and pTi200 & pTiMAO200 and pTi400 & pTiMAO400 at 4 h ($p < 0.05$). Generally, the cell adhesion ratio on the pTi group seems to be lower than that on the pTiMAO group. These results indicate that formation of the MAO coating on the pTi benefits the MC3T3-E1 cell adhesion after culturing for 0.5−4 h different from formation of the MAO coating on Ti.

(4) In Ti-MAO & pTiMAO groups: The cell adhesion ratio on Ti-MAO is higher than that on pTiMAO200 ($p < 0.05$) and similar to that of the other samples in the pTiMAO group after culturing for 0.5 h. After culturing for 1 h, however, the difference in the cell adhesion ratio between Ti-MAO and pTiMAO is not obvious. Interestingly, with increasing culturing time, the cell adhesion ratio on Ti-MAO is lower than that on pTiMAO, such as Ti-MAO & pTiMAO400 at 2 h ($p < 0.05$) and Ti-MAO & pTiMAO100 and Ti-MAO & pTiMAO400 at 4 h ($p < 0.05$). These results indicate that the pTiMAO group shows good MC3T3-E1 cell adhesion at the later stage of cell culture, although it exhibits a lower cell adhesion ratio at the early stage of cell culture compared to Ti-MAO.

(5) In pTi or pTiMAO groups: The difference in the cell adhesion ratio on some samples of the pTi or pTiMAO groups was observed after culturing for 0.5, 1, and 2 h. After culturing for 0.5 h, the difference in the adhesion ratio occurs among (pTi100 and pTi600), pTi200, and pTi400 of the pTi group. At this time, a similar difference in the cell adhesion ratio also is found in the pTiMAO group. After culturing for 1 h, the difference in the adhesion ratio occurs between pTi200 and pTi600 in the pTi group. At this time in the pTiMAO group, pTiMAO400 shows a higher cell adhesion ratio compared to pTiMAO200 and pTiMAO600. After culturing for 2 h, pTi400 and pTiMAO400 both show a higher cell adhesion ratio compared to the other samples respectively in the pTi and pTiMAO groups. However, the difference in the cell adhesion ratio of the samples in the pTi or pTiMAO group is not obvious after culturing for 4 h. These results indicate that the microbead size has an effect on the cell adhesion ratio at the early stage of cell culture.

3.3.4. Cell Proliferation. Figure 6 shows the cell proliferation number on the surfaces of the four groups (Ti, Ti-MAO, pTi, and pTiMAO).

(1) In Ti & pTi groups: The Ti and pTi groups show the cell proliferation number at similar levels after culturing for 1 day, except that of pTi100 is lower than that of Ti ($p < 0.05$). After culturing for 4 days, the Ti and pTi groups show the cell proliferation number at similar levels, except that of pTi600 is higher than that of Ti ($p < 0.05$). After culturing for 7 days, it was interesting that the MC3T3-E1 cell numbers on pTi increase very quickly and show higher cell proliferation number compared to Ti ($p < 0.05$). After culturing for 10 days, the MC3T3-E1 cell proliferation number on pTi is still greatly higher than that on Ti ($p < 0.05$). These results indicate that the macropore of pTi does not benefit cell proliferation at the early stage of cell culture such as 1 day; however, it highly benefits cell proliferation at the later stage of cell culture compared to Ti.

(2) In Ti & Ti-MAO groups: The cell proliferation number on Ti-MAO is obviously higher than that on Ti ($p < 0.05$) after culturing for 1, 4, 7, and 10 days, indicating that formation of the MAO coating on Ti greatly increases the cell proliferation number. In addition, after culturing for 10 days, the change in the MC3T3-E1 cell proliferation on Ti-MAO is not evident compared to culturing for 7 days, suggesting a saturated cell proliferation number. However, the MC3T3-E1 cell numbers on Ti decrease ($p < 0.05$), suggesting death of the MC3T3-E1 cells.

(3) In pTi & pTiMAO groups: The cell proliferation number on the pTiMAO group is lower than that on the Ti-MAO group ($p < 0.05$) after culturing for 1 day. After culturing for 4 days, the number on Ti-MAO is higher than that on the samples in the pTiMAO group ($p < 0.05$) except that of pTiMAO100 is similar to that of Ti-MAO. After culturing for 7 days, the cell proliferation number on Ti-MAO is higher than that on pTiMAO400 and pTiMAO600 ($p < 0.05$); however, the numbers on pTiMAO100 and pTiMAO200 are both similar to that on Ti-MAO. After culturing for 10 days, the

difference in the cell proliferation number on Ti-MAO and pTiMAO is not obvious. These results indicate that the macropore of pTiMAO does not benefit cell proliferation at the early stage of cell culture similar to the comparison between Ti and pTi.

(4) In Ti-MAO & pTiMAO groups: By comparison with the pTi and pTiMAO groups, cell proliferation on both pTiMAO100 and pTiMAO400 is higher than that on pTi100 and pTi400 ($p < 0.05$) after cell culturing for 1 day. After culturing for 4 days, the cell proliferation number on the pTiMAO group is obviously higher than that on the pTi group ($p < 0.05$). After culturing for 7 days, the cell proliferation number on both pTi100 and pTi400 is higher than that on pTiMAO100 and pTiMAO400 ($p < 0.05$). After culturing for 10 days, the cell proliferation number on pTi100 is still higher than that on pTiMAO100 ($p < 0.05$). These results reveal that formation of the MAO coating on pTi increases the MC3T3-E1 cell proliferation number at the early stage of cell culture.

(5) In pTi or pTiMAO groups: Certainly, the differences in the MC3T3-E1 cell proliferation number on the samples in the pTi group as well as the pTiMAO group are found after culturing for 1, 4, and 7 days. However, this difference is not obvious after culturing for 10 days. For example, it is found in the pTi group that the cell proliferation number on pTi100 is lowest after cell culturing for 1 day ($p < 0.05$). However, it changes to the most after culturing for 7 days ($p < 0.05$). These results indicate that cell proliferation on the samples in the pTi group are different during the cell culture period, depending on the microbead size of the samples in the pTi group. In fact, the effect of the Ti microbead diameter on the cell proliferation number is also observed on the samples in the pTiMAO group, especially at the early stage of the cell culture.

Figure S1 in the Supporting Information (SI) shows the typical SEM morphology of cell proliferation on pTi100 and pTiMAO100 after culturing for 4 days. It is found that many MC3T3-E1 cells are at the connection region by Ti microbeads, as shown by white arrows. Of course, besides the connection region, some MC3T3-E1 cells also are observed at the top or side of the microbeads. Similar results are observed on the other samples in the pTi and pTiMAO groups (not shown here).

3.3.5. ALP Activity of the Cell. Figure 7 shows the ALP activity of the MC3T3-E1 cell culturing for 3 days on the surfaces of the four groups of Ti, pTi, Ti-MAO, and pTiMAO. The ALP activity of cells on Ti is higher than that on pTi200 and pTi600 ($p < 0.05$) and similar to that on pTi100 and pTi400. This result indicates that the macroporous structure could decrease the ALP activity of the cells after culturing for 3 days. Compared to Ti, the ALP activity of cells on Ti-MAO is at a similar level, suggesting that formation of the MAO coating on Ti has no effect on the ALP activity of cells after culturing for 3 days. Compared to Ti-MAO, no difference in the ALP activity of cells on pTiMAO100 and pTiMAO400 is observed; however, that on pTiMAO200 and pTiMAO600 is lower than that on Ti-MAO ($p < 0.05$).

In the pTi group, the ALP activity of cells on pTi400 is higher than that on pTi100, and these two samples are both higher than that on the pTi200 and pTi600 samples ($p < 0.05$). In the pTiMAO group, the ALP activity of cells on pTiMAO100 is similar to that on pTiMAO400, and these two samples are both still higher than that on the pTi200 and pTi600 samples ($p < 0.05$). The high ALP activity of cells on the pTi and pTiMAO groups has a selective feature after cell culturing for 3 days, depending on the macroporous structure of the samples in the pTi and pTiMAO groups. These results indicate that the cell response is highly sensitive to the shape of the substrates.

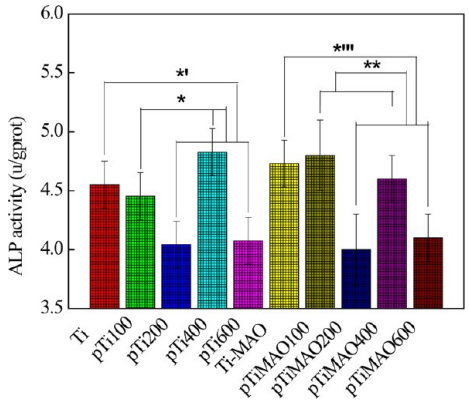

Figure 7. ALP activity of cells culturing for 3 days on the surfaces of each sample in the four groups of Ti, pTi, Ti-MAO, and pTiMAO. Note: * means the comparison among the samples in the pTi group; ** means the comparison among the samples in the pTiMAO group; *′ means the comparison with Ti and the samples in the pTi group; *‴ means the comparison with Ti-MAO and the samples in the pTiMAO group; *, **, *′, and *‴ represent $p < 0.05$. The software of *SAS6.0* was used to perform statistical analysis, and the sample number of each material is more than 8.

3.3.6. Ion Release. Recent studies indicate that the cell response is related to elemental release from the material surface.[26−28] Figure S2 in the SI shows the change in the Ca and Si atomic concentrations on the sample surfaces in the Ti-MAO and pTiMAO groups during cell culturing for different times. Elemental dissolution is observed on all surfaces of the Ti-MAO and pTiMAO groups. The previous research indicates that the Ca and Si concentrations of the pTiMAO group increase with increasing microbead diameter from 100 to 400 μm and then decrease with increasing microbead diameter to 600 μm.[23] In this work, it can be seen that the atomic concentrations of the released Ca and Si show similar changes, depending on the microbead diameter.

3.4. In Vivo Animal Investigation. *3.4.1. Radiographic Evaluation.* X-ray is used to evaluate osseointegration between the implants and surrounding bone tissues. Figure 8 shows the typical sagittal and coronal radiographs of the pTi and pTiMAO samples after implantation for 4 and 8 weeks. The pTi and pTiMAO implants remain at the initial implanting locations in the rabbit tibia, and no evident loosening or dislocation is observed after implantation for 4 and 8 weeks. No fractures of the pTi and pTiMAO implants as well as the tibia are observed in these radiographs, although the implants occupy a major proportion of the weight-bearing bone structures in the tibias. After implantation for 4, 8, and 12 weeks, when the rabbits are sacrificed, the implants still exhibit good fusion with the surrounding bone tissues.

3.4.2. Micro-CT Images. Using a micro-CT technique can distinguish three phases of bone (100−1524 HU), soft tissue (23−100 HU), and implant (>1524 HU). During the micro-CT experiment, X-ray is used to acquire images for the composition and structure information of the materials. When X-ray penetrates the samples, absorption in X-ray by the materials will appear and thus the intensity of the transmitting X-ray decreases. Changes in the intensity of the transmitting X-

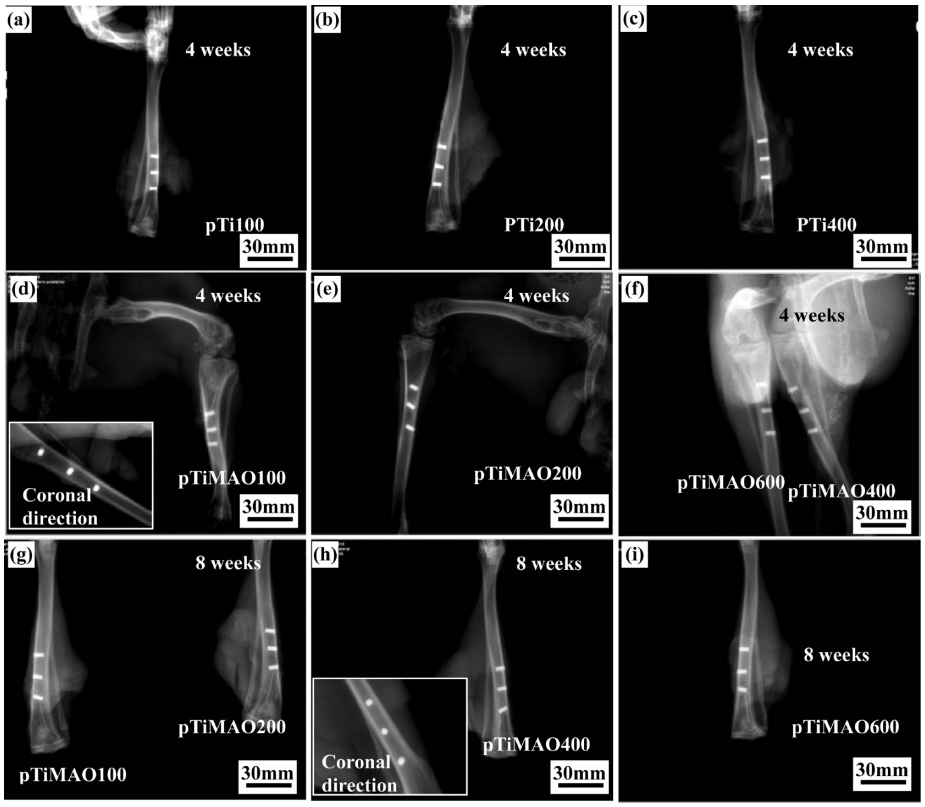

Figure 8. Sagittal and coronal radiographs of the pTi and pTiMAO implants after implantation in the rabbit tibia for 4 and 8 weeks: (a) pTi100, (b) pTi200, and (c) pTi400 for 4 weeks; (d) pTiMAO100, (e) pTiMAO200, and (f) pTiMAO400 and pTiMAO600 for 4 weeks; (g) pTiMAO100 and pTiMAO200, (h) pTiMAO400, and (i) pTiMAO600 for 8 weeks.

ray can produce images with different gray levels, which reflects the composition, thickness, density, and so on of the materials. The micro-CT technique is an important method to observe bone growth and evaluate various scaffolds for the bone tissue engineering area.

Figure S3 in the SI shows the typical micro-CT images on a gray scale of the pTiMAO implants after implantation for 12 weeks observed with one direction. These images clearly confirm that the four kinds of pTiMAO implants do not cause any adverse effects after implantation for 12 weeks. At the same time, it was notable that continuous bones are around the pTiMAO implants and they cover the implants completely and perfectly (see Figure S3 in the SI).

Figure 9 shows the micro-CT-colorized images for the pTiMAO implants in different viewing directions after implantation for 12 weeks. In Figure 9, the micro-CT images clearly demonstrate the different viewing directions for the growth of new bones. Normally, implants are blue (outer region) and green (inner region), soft tissues are purple, and bones are orange. Because of the different absorptions in X-ray by these phases and the scattering from metals, the images sometimes could be interrupted.[4,29] Thus, a thin layer of noise could appear around the boundary of the implant edge.[4,29]

However, the implantation results in this work can still be analyzed clearly by the current micro-CT images. Little region with orange in the interior of the pTiMAO100 implant is observed in the front and top views of Figure 9a because of the formation of new bones in the macropores in the pTiMAO100 implant. The surface of the pTiMAO100 implant obviously shows the formation of new bones, as shown by white arrows in Figure 9a. In addition, a thin layer of soft tissue is observed at the surface of the newly formed bones, as shown by green arrows in the front and top views of Figure 9a. This soft tissue is combined with the host soft tissue, which forms a continuous structure covered on the inner wall of the bone cavity. In the pTiMAO200, pTiMAO400, and pTiMAO600 implants, the newly formed bones are very remarkable. Even, the regions with orange are also observed at the right end of the pTiMAO implants, suggesting formation of the new bones at these regions and indicating very good osseointegration in vivo. Namely, the interconnected macropores in the pTiMAO implants form a three-dimensional porous space, in which the new bones can grow freely. According to these results, the pTiMAO implants can provide a large space for bone growth.

Around the pTiMAO implants, the new bones have good continuity with the surrounding host bones such as the side view. In these images, no cracks are observed at the interface between the pTiMAO implants and new bones. Thus, good mechanical property matching can be produced between the pTiMAO implants and new bones. In other words, the macroporous structure of the pTiMAO implants can effectively absorb the force created by the loading and unloading. In a word, the micro-CT evaluation clearly distinguishes the phases of the macroporous implants, the host and the new bones, and the soft tissue, clearly showing good implantation status and their interconnected relationship.

Table 2 shows the porosity of the pTiMAO implants and the volume ratio of the new bone in the macropores of the pTiMAO samples after implantation for 12 weeks. It can be seen that the porosity of the pTiMAO samples and the volume ratios of the new bone increase with increasing microbead diameter. Because of the higher porosity and bioactivity with

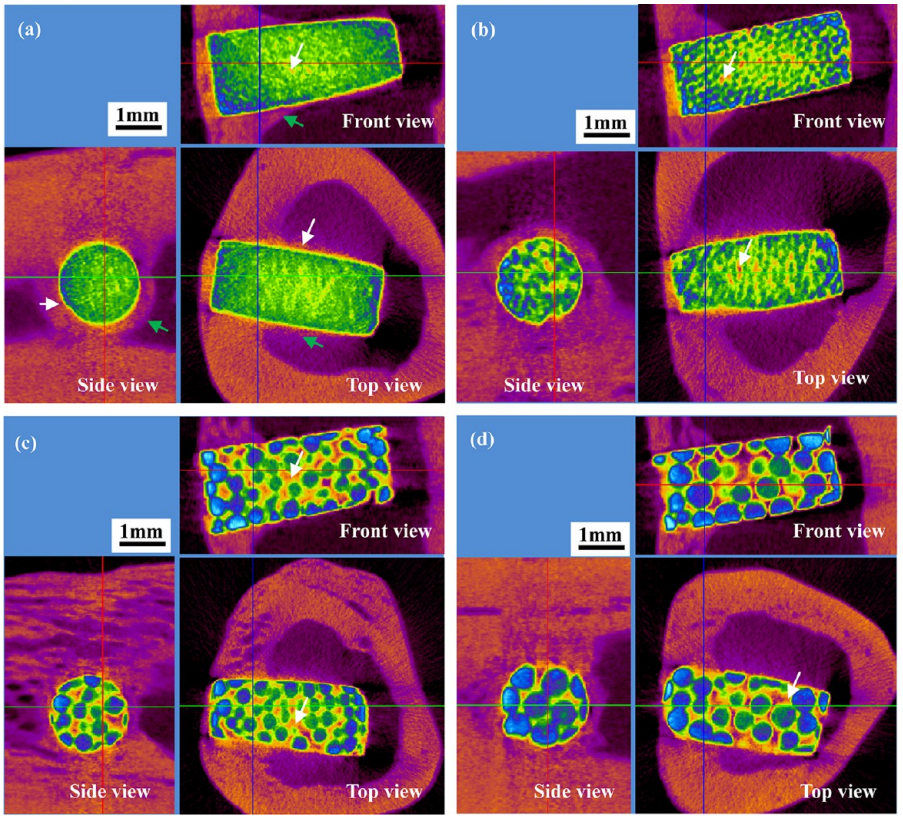

Figure 9. Micro-CT images in three directions for viewing the pTiMAO implants after implantation in the rabbit tibia for 12 weeks: (a) pTiMAO100; (b) pTiMAO200; (c) pTiMAO400; (d) pTiMAO600 (blue and green for the outer and inner implants, purple for soft tissues, and orange for bone). Note: the new bones are marked by white arrows, and soft tissues are marked by green arrows.

Table 2. Porosity of the pTiMAO Implants and the Volume Ratios of the New Bone in the Macropores of the pTiMAO Samples after Implantation for 12 Weeks

sample	porosity[23] (%)	ratio for new bone and implants[a] (%)	ratio for new bone and macropores[b] (%)
pTiMAO100	26.5	19.5	74
pTiMAO200	30.5	25	82
pTiMAO400	34	30	88
pTiMAO600	35	31	89

[a]Percentage for the new bone volume occupying the implant volume. [b]Percentage for the new bone volume occupying the macropore volume.

increasing microbead diameter, higher ratios for the new bone volume and macropore volume are observed, suggesting that osseointegration of the pTiMAO implants with larger macropore size could benefit bone formation in this work.

3.4.3. SEM Observation and EDS Analysis of the Pushed-Out Implants. Figure 10 shows the SEM morphology and EDS results of the pulled-out Ti, Ti-MAO, and pTiMAO implants after implantation in the rabbit tibia for 4, 8, and 12 weeks. After implantation for 4 weeks, the sound Ti, Ti-MAO, and pTiMAO implants are observed after pushing out, as shown in Figure 10a–e. The surfaces of the implants such as pTiMAO100 are covered by the roughness bone tissues, as shown in Figure 10f, and the initial macropores of pTiMAO100 basically are filled with the newly formed bones according SEM and EDS analysis (EDS not shown here). Similar results are found in the other pTiMAO implants. In addition, the end of pTiMAO400 that locates at the marrow cavity place of the tibia is broken purposely to detect the newly formed bone, as shown by the white arrows in Figure 10d, and the SEM and EDS results indicate the appearance of the newly formed bone (EDS not shown here).

After implantation for 8 weeks, the sound Ti, Ti-MAO, pTiMAO100, pTiMAO200, and pTiMAO400 implants are obtained after pushing out except one pTiMAO600 implant, which is broken off. In addition, the end of pTiMAO400 that locates at the marrow cavity place of the tibia is also purposely broken to detect the newly formed bone, as shown by the white arrows in Figure 10j. Of course, the newly formed bones are found according to the SEM and EDS results, which shows the appearance of Ca and P elements in Figure 10l. After pushing out the pTiMAO600 implants, one pTiMAO600 implant is fractured and the newly formed bones still remain on the pTiMAO600 implant. This result indicates that the interface bonding strength between the newly formed bone and the implant is very high.

After implantation for 12 weeks, except two pTiMAO600 implants, which are broken off after pulling out, the other implants are sound. In addition, the large block bones remain on the end of the pTiMAO400 and pTiMAO600 implants, suggesting a high interface bonding strength between the newly formed bone and the implants.

Figure S4 in the SI shows the surface morphology and EDS results of pTiMAO400 after implantation for 8 weeks. It is observed that many micropores of pTiMAO400 are filled with new compounds. According to the EDS results like point A, it is surprising that the newly formed compound in the micropore contained lots of C, O, Ca, and P elements, which indicates that the newly formed bone tissues can form in the micropores of

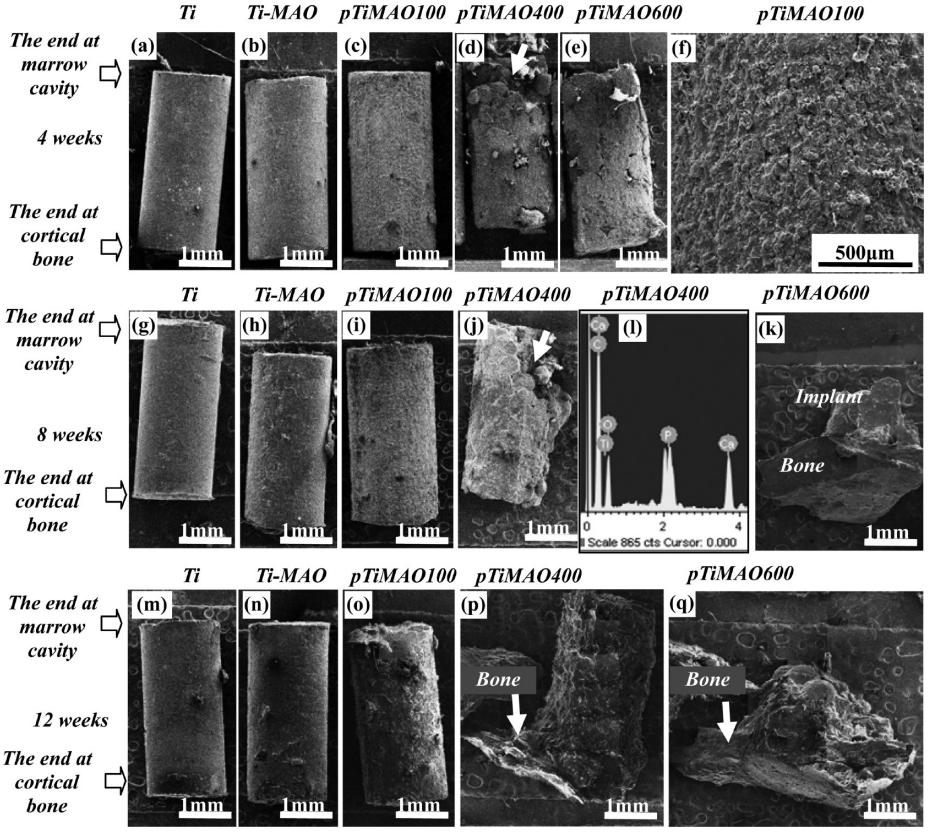

Figure 10. SEM morphology and EDS results of the pushed-out Ti, Ti-MAO, and pTiMAO implants after implantation for 4, 8, and 12 weeks: (a) Ti, (b) Ti-MAO, (c) pTiMAO100, (d) pTiMAO400, (e) pTiMAO600, and (f) pTiMAO100 under higher magnification after implantation for 4 weeks; (g) Ti; (h) Ti-MAO; (i) pTiMAO100; (j) pTiMAO400; (l) EDS for the new bone in the macropore of pTiMAO400 at the place shown by a white arrow in part j; (k) pTiMAO600 after implantation for 8 weeks; (m) Ti, (n) Ti-MAO, (o) pTiMAO100, (p) pTiMAO400, and (q) pTiMAO600 after implantation for 12 weeks. Note: the new bones in the macropore and around the implants are marked by white arrows.

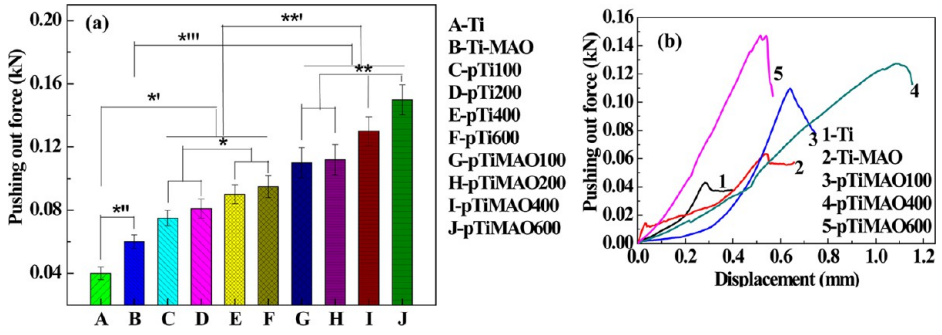

Figure 11. Pushing-out force and displacement curves for the Ti, pTi, Ti-MAO, and pTiMAO implants after implantation for 12 weeks: (a) pushing-out force; (b) displacement curves. Note: * means the comparison among the samples in the pTi group; ** means the comparison among the samples in the pTiMAO group; *′ means the comparison with Ti and the samples in the pTi group; *″ means the comparison with Ti and the samples in the Ti-MAO; *‴ means the comparison with Ti-MAO and the samples in the pTiMAO group; **′ means the comparison with the samples in the pTi group and the samples in the pTiMAO group.*, **, *′ ,*‴, and **′ represent $p < 0.05$. The software of *SAS6.0* was used to perform statistical analysis, and the sample number of each material is more than 6.

pTiMAO400. Moreover, a similar phenomenon is observed on the other surfaces of the Ti-MAO and pTiMAO implants.

3.4.4. Measurement of the Pushing-Out Force and Displacement Curves. Figure 11a shows the pushing-out force for the Ti, pTi, Ti-MAO, and pTiMAO implants after implantation for 12 weeks. The pushing-out force for the Ti implant is about 40 N, while that for the Ti-MAO implant is enhanced by 50% to about 60 N ($p < 0.05$). Then, the pTiMAO implants display greater improvement in the pushing-out force compared to Ti-MAO. It is found that the pushing-out forces for pTiMAO100 and pTiMAO200 are nearly 3 times that for the Ti implant ($p < 0.05$) and nearly 2 times that for the Ti-MAO implant ($p < 0.05$). With respect to pTiMAO400 and pTiMAO600, the pushing-out forces for the two implants further increase. At the same time, it is noticed that the pushing-out force for pTi is obviously higher than that of Ti, and it is obviously lower than that of pTiMAO. These results indicate that the macroporous structure and formation of the MAO coating could significantly improve the pushing-out force and benefit osseointegration of the implants.

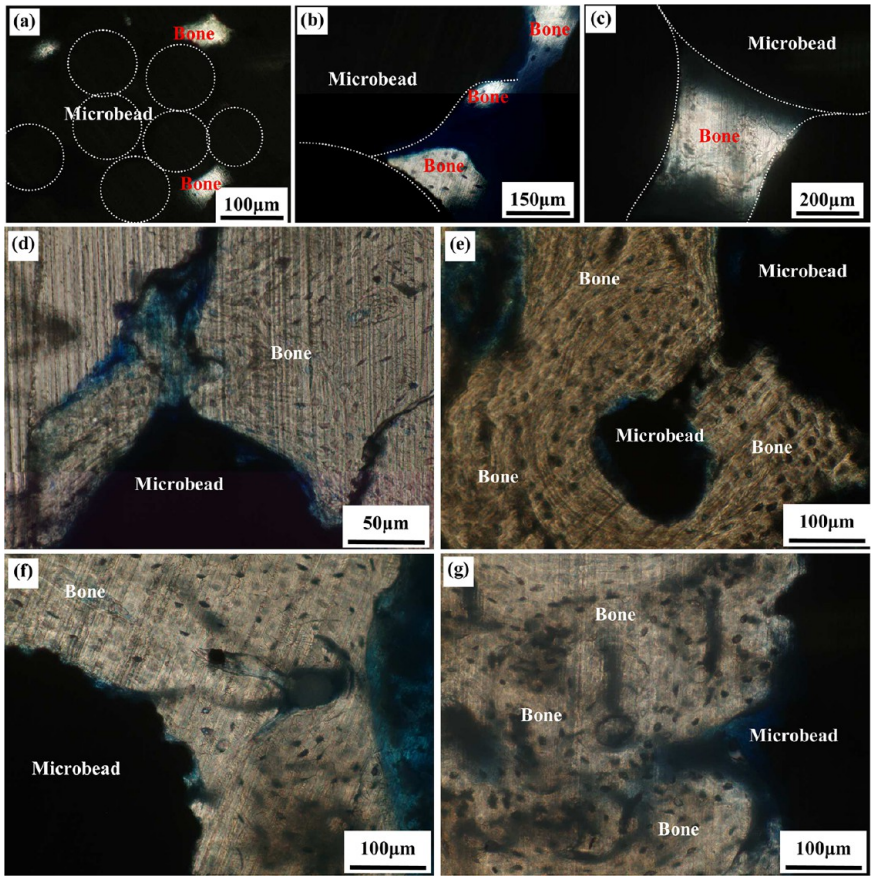

Figure 12. Histological analysis of bone tissues on the pTiMAO group after implantation for 12 weeks in the rabbit tibia: (a–c) formation of the bone tissues in the interior of pTiMAO100, pTiMAO400, and pTiMAO600 near the ends of the implants that do not contact the host bones; higher magnification for (d) pTiMAO100, (e) pTiMAO200, (f) pTiMAO400, and (g) pTiMAO600 near the ends of the implants at the implanting sites.

Figure 11b shows the typical displacement curves during the pushing-out tests. It is notable that the maximum displacement for Ti, Ti-MAO, pTiMAO100, and pTiMAO400 obviously increases in sequence. Especially, the maximum displacement of pTiMAO400 (about 1.1 mm) is greatly higher than those of the other implants. In addition, an interesting phenomenon is that the maximum displacement of pTiMAO600 decreases compared to that of pTiMAO400.

3.4.5. Histological Analysis. Figure 12 shows histological analysis of the bone tissues on the pTiMAO implants after implantation for 12 weeks in the rabbit tibia. Parts a–c of Figure 12 show that the new bone tissues form in the inner macropores of the pTiMAO implants at the marrow cavity place of the rabbit tibia. These results indicate good osseointegration of the pTiMAO implants. However, in pTiMAO100, the new bones do not completely grow into the macropores of the implant at the marrow cavity location, as shown in Figure 12a.

Parts d–g of Figure 12 show the higher magnification images for the interface bonding between the newly formed bones and the implants at the places of the cortical bone. No adverse effects and no apparent gaps are observed at the interfaces between the implants and new bone. Osteoblasts are distributed uniformly in the newly formed bones.

4. DISCUSSION

4.1. Structure of the MAO Coatings. The previous results showed that the surface morphology, elemental composition, and phase composition of the MAO coatings on the macroporous Ti sintered by microbeads are significantly affected by the microbead diameter.[23,24] Moreover, the porosity of macroporous Ti gradually rises in the range of 26.5–35%, and the specific surface area of macroporous Ti decreases gradually in the range of 45–5% mm^{-1} with increasing titanium microbead diameter.[23] The porosity and specific surface area are two key factors influencing the formation and microstructures of the MAO coatings. Because of this, the pTiMAO samples have higher Ca and Si elemental concentrations compared to the Ti-MAO sample. The different elemental concentrations can influence the cell response because of the different surface charge and ion dissolution. With respect to the phase composition, the results reveal that the amorphous phase with Si, Na, Ca, Ti, and O elements is the major phase of the pTiMAO samples except of a few TiO_2 nanocrystals.

4.2. Cell Response. The effects of the Ti and Ti-MAO coatings on the cell response are discussed in recently published research.[25] This work focuses on the cell response on pTi and pTiMAO. The current results indicate that cell attachment on pTi and pTiMAO indicates relationships with their space structures. Surely, the MC3T3-E1 cells can locate the connection region among microbeads, especially when the microbead diameter is small. The reason for this probably is related to the shape of the microbeads and cell spreading. Most research on cell attachment is conducted on the plate plane.[26,27,30–45] The attachment of the MC3T3-E1cells on the spherical surface could become difficult in a short time in

0.5−4 h. SEM observations indicate that the MC3T3-E1 cells show flat morphology after final cell attachment. Formation of the flat morphology should be easier on the plate plane compared to the spherical surface. The MC3T3-E1 cells are apt to spread with flat morphology at the connection region by the microbeads. These cells contact two microbeads through extension of their pseudopodia, as shown in Figure 3a. On the other hand, the curvature or landform of the connection region could be different from that of the other regions, as shown in Figure 3a, which could not relatively benefit cells to spread with flat morphology. Thus, MC3T3-E1 cells can distribute at the connection regions, when the microbead diameter is small. This adhesion status could produce a problem that the cell adhesion speed could decrease compared to the flat plane. This may be the reason why the cell attachment number on the pTi group is lower than that on the Ti sample after cell culturing for 0.5−4 h because only some MC3T3-E1 cells could adhere to the connection region among the microbeads.

At the early stage of cell adhesion, the cell adhesion ratio decreases in the following sequence: Ti, Ti-MAO, pTiMAO, and pTi. The cell adhesion ratio on Ti-MAO decreases compared to Ti because of formation of the MAO coatings. This could be related to the effect of the chemical composition on the MAO coating.[28] The cell adhesion ratio on pTiMAO is lower than that on Ti-MAO, which is probably due to the effect of the macroporous structure as mentioned above. However, it is found that the cell adhesion ratio on pTiMAO is higher than that on pTi. Formation of the MAO coating on pTi improves the cell adhesion ratio, which is different from the comparison with Ti and Ti-MAO. Formation of the MAO coating on pTi could change the surface topology of the connection region and the cells could relatively easily adhere at this region because of the effect of the micropores on the MAO coatings compared to pTi. At the later stage of cell adhesion, the cell adhesion ratio decreases in the following sequence: pTiMAO, Ti-MAO similar to Ti, and pTi. Compared to Ti-MAO, the higher cell adhesion ratio of pTiMAO is related to the chemical composition, which is discussed as follows.

The previous results indicate that the effect of the chemical composition of the MAO coatings on MC3T3-E1 cell attachment is pronounced.[28] The addition of Ca and Si elements on the surface of Ti by MAO or other surface modification methods such as ion implantation could give rise to a specially altered surface charge, which could further influence cell attachment.[27] Thus, attachment of the MC3T3-E1 cells on the Ti-MAO sample was prolonged compared to that of the Ti sample based on this and previous research.[28]

Compared to Ti-MAO, the attachment ratio of the MC3T3-E1 cells on the pTiMAO group increases after culturing for 4 h, although the space structure could decrease cell attachment at this culture stage according to the above discussion. This should imply that the other factor could influence attachment of the MC3T3-E1 cells on the pTiMAO group. Previous research indicates that the appropriate concentrations of Si and Ca released from the Ti-MAO sample could benefit cell attachment.[28] Of course, slightly released concentrations of Si and Ca could not affect cell attachment and great release could decrease the cell attachment ability because of their toxicity.[26,28] We consider that the released concentrations of Ca and Si from the pTiMAO group at cell culturing for 4 h are more suitable for cell attachment compared to those from Ti-MAO.

However, according to the current results, the released Ca and Si concentrations from the pTiMAO group are higher than those from the Ti-MAO group after cell culturing for 1, 4, and 7 days. Surely, lots of the released Ca and Si could give rise to damage of the cell proliferation as mentioned above, which is different from that at the early stage of cell culturing for 4 h. Of course, this decrease in cell proliferation at higher released Ca and Si concentrations is relative to the suitable concentration. Thus, after cell culturing for 1, 4, and 7 days, cell proliferation on the pTiMAO group is lower than that on the Ti-MAO sample.

On the other hand, the space structure was believed to improve cell proliferation. After cell culturing for 4, 7, and 10 days, the cell proliferation number on the pTi group is significantly higher than that on the Ti sample. These results indicate that the space structure could increase cell proliferation. With increasing culturing time, lots of connection regions especially in the interior of the pTi group could provide positions for cell attachment and proliferation. At the same time, cell attachment also appears on the top and side of the microbeads besides the connection regions after culturing for a long time because of interaction between the cells and substrate. Thus, the larger surface area is provided by the pTi group for cell proliferation with increasing culturing time. Also, it is noticed that the cell proliferation number on the pTiMAO group is lower than that on the pTi group after cell culturing for 7 days. The reason for this is that the high concentration of the released Ca and Si elements could further decrease cell proliferation. At the same time, the cell proliferation number on pTiMAO is similar to that on Ti-MAO after culturing for 10 days, which is probably due to the enhancement effect of the space structure.

4.3. Osseointegration and Biomechanical Properties of pTiMAO in Vivo. The radiographs, micro-CT images, and histological analysis indicate that no adverse effects such as inflammatory reactions appear at the interface between the implants and newly formed bones. No apparent gap is found at the interface between the implants and newly formed bones. These results indicate that all implants have very good biocompatibility. The new bones were formed in the micropores of the MAO coatings after implantation (see Figure S4 in the SI). The new bone formation process in the micropores is caused by the functions of bone cells and the deposition of Ca and P elements resulting from the bioactivity of the MAO coatings containing Ca, Si, and Na.[25] At the same time, the newly formed bone tissues also completely grow into the macropores of the pTiMAO implants according to SEM, EDS, and histological analysis. These results indicate that the pTiMAO implants have very good osseointegration ability.

According to the radiographs and micro-CT images, all implants remain in the rabbit tibia at the initial implanting locations and no evident loosening or dislocation is observed after implantation for 4, 8, and 12 weeks. These results indicate that all implants could connect bones well. Both X-ray and micro-CT images show that the bone tissues are around the surfaces of the pTiMAO implants. Moreover, no fractures of the implants and tibia are observed in the radiographs and micro-CT images. These results suggest that the current implants were compatible in vivo in their biomechanical properties. Furthermore, no damage of the MAO coatings is observed after implantation for 4, 8, and 12 weeks, suggesting that the interface bonding between the MAO coatings and Ti is very good.

Previous research demonstrates the factors that contribute to the improvement in the biomechanical properties according to comparison with Ti and Ti-MAO.[25] In this work, the pushing-out forces of the pTiMAO samples are higher than those of the Ti-MAO implant, and they increased with increasing microbead diameter. The change in the pushing-out force is related to the following factors. First, the Ca and Si concentrations increase with increasing microbead diameter,[23] which could benefit the new bone formation and improve the pushing-out force because of improvement of the bioactivity. On the other hand, the mechanical properties of the pTi samples decrease with increasing microbead diameter according to previous research.[22] The pushed-out Ti, Ti-MAO, pTiMAO100, pTiMAO200, and pTiMAO400 samples are not broken after implantation for 4, 8, and 12 weeks. However, some of the pushed-out pTiMAO600 samples are broken after implantation for 8 and 12 weeks, suggesting the compressive strength of pTiMAO600 is near the interface bonding strength between the new bones and pTiMAO600 implant.

Furthermore, it is notable that displacement for Ti, Ti-MAO, pTiMAO100, and pTiMAO400 obviously increases because of increasing interface bonding strength. However, displacement of the pTiMAO600 implant decreases compared to that of the pTiMAO400 implant. As mentioned above, the porosity of the macroporous Ti rises gradually with increasing microbead diameter, and new bones could grow into the macropores of the pTiMAO implants, which suggests that more new bones can be formed in pTiMAO600. Thus, the mechanical properties of the pTiMAO600 implant could be near those of bones. Therefore, the new bones in the macropores of the pTiMAO600 implant have an important effect on displacement.

5. CONCLUSION

Bioactive MAO coatings containing lots of the amorphous phase with Si, Ca, Ti, Na, and O elements and few TiO_2 nanocrystals are prepared on the macroporous Ti sintered by Ti microbeads. The particular space structures of pTi and pTiMAO as well as the chemical composition of the MAO coatings have important effects on the adhesion, proliferation, and ALP activity of the MC3T3-E1 cells. The macropores of the implants do not benefit cell attachment; however, they significantly enhance cell proliferation. Ti, Ti-MAO, and pTiMAO did not give rise to any adverse reactions in vivo. In addition, the MAO coatings show good interface bonding with new bones as well as implants. Furthermore, pTiMAO could provide a large space for bone growth, showing perfect osseointegration and greatly enhancing the bonding strength between the implants and new bones by mechanical interlocking, especially with pTiMAO400, showing good deformation during the pushing-out experiment.

■ ASSOCIATED CONTENT

Supporting Information

SEM image for proliferation of the MC3T3-E1 cells on pTi100 and pTiMAO100, change in the Ca and Si atomic concentrations on the sample surfaces, micro-CT images in gray scale of the pTiMAO implants after implantation, and EDS results of the compound in the micropores. This material is available free of charge via the Internet at http://pubs.acs.org.

■ AUTHOR INFORMATION

Corresponding Author

*Tel: +86-451-8640-2040-8403. Fax: +86-451-8641-4291. E-mail: daqingwei@hit.edu.cn.

Notes

The authors declare no competing financial interest.

■ ACKNOWLEDGMENTS

This work was financially supported by the National Basic Science Research Program (Grant 2012CB933900), National Natural Science Foundation of China (Grants 51002039 and 51021002), Fund for the Doctoral Project to new teachers, and the Fundamental Research Funds for the Central Universities (Grant HIT.NSRIF.2014002).

■ REFERENCES

(1) Melican, M. C.; Zimmerman, M. C.; Dhillon, M. S.; Ponnambalam, A. R.; Curodeau, A.; Parsons, J. R. Three-Dimensional Printing and Porous Metallic Surfaces: a New Orthopedic Application. *J. Biomed. Mater. Res.* **2001**, *55*, 194−202.

(2) Li, J. P.; Habibovic, P.; van den Doel, M.; Wilson, C. E.; de Wijn, J. R.; van Blitterswijk, C. A.; de Groot, K. Bone Ingrowth in Porous Titanium Implants Produced by 3D Fiber Deposition. *Biomaterials* **2007**, *28*, 2810−2820.

(3) Ryan, G.; Pandit, A.; Apatsidis, D. P. Fabrication Methods of Porous Metals for Use in Orthopaedic Applications. *Biomaterials* **2006**, *27*, 2651−2670.

(4) Liu, X. M.; Wu, S. L.; Yeung, K. W. K.; Chan, Y. L.; Hu, T.; Xu, Z. S.; Liu, X. Y.; Chung, J. C. Y.; Cheung, K. M. C.; Chu, P. K. Relationship between Osseointegration and Superelastic Biomechanics in Porous NiTi Scaffolds. *Biomaterials* **2011**, *32*, 330−338.

(5) Nguyen, H. Q.; Deporter, D. A.; Pilliar, R. M.; Valiquette, N.; Yakubovich, R. The Effect of Sol−Gel-Formed Calcium Phosphate Coatings on Bone Ingrowth and Osteoconductivity of Porous-Surfaced Ti Alloy Implants. *Biomaterials* **2004**, *25*, 865−876.

(6) Frayssinet, P.; Trouillet, J. L.; Rouquet, N.; Azimus, E.; Autefage, A. Osseointegration of Macroporous Calcium Phosphate Ceramics Having a Different Chemical Composition. *Biomaterials* **1993**, *14*, 423−429.

(7) Rubshtein, A. P.; Trakhtenberg, I. Sh.; Makarova, E. B.; Triphonova, E. B.; Bliznets, D. G.; Yakovenkova, L. I.; Vladimirov, A. B. Porous Material Based on Spongy Tianium Granules: Structure, Mechanical Properties, and Osseointegration. *Mater. Sci. Eng., C* **2014**, *35*, 363−369.

(8) Aguilar Maya, A. E.; Grana, D. R.; Hazarabedian, A.; Kokubu, G. A.; Luppo, M. I.; Vigna, G. Zr−Ti−Nb Porous Alloys for Biomedical Application. *Mater. Sci. Eng., C* **2012**, *32*, 321−329.

(9) Oh, I. H.; Nomura, N.; Masahashi, N.; Hanada, S. Mechanical Properties of Porous Titanium Compacts Prepared by Powder Sintering. *Scr. Mater.* **2003**, *49*, 1197−1202.

(10) Murray, G. A.; Semple, J. C. Transfer of Tensile Loads from a Prosthesis to Bone Using Porous Titanium. *J. Bone Joint Surg. Br.* **1981**, *63-B*, 138−141.

(11) Cheng, S.; Wei, D. Q.; Zhou, Y.; Guo, H. F. Characterization and Properties of Microarc Oxidized Coatings Containing Si, Ca and Na on Titanium. *Ceram. Int.* **2011**, *37*, 1761−1768.

(12) Yerokhin, A. L.; Nie, X.; Leyland, A.; Matthews, A.; Dowey, S. J. Plasma Electrolysis for Surface Engineering. *Surf. Coat. Technol.* **1999**, *122*, 73−93.

(13) Sundararajan, G.; Krishna, L. R. Mechanisms Underlying The Formation of Thick Alumina Coatings through The MAO Coating Technology. *Surf. Coat. Technol.* **2003**, *167*, 269−277.

(14) Tian, J.; Luo, Z. Z.; Qi, S. K.; Sun, X. J. Structure and Antiwear Behavior of Micro-Arc Oxidized Coatings on Aluminum Alloy. *Surf. Coat. Technol.* **2002**, *154*, 1−7.

(15) Cheng, S.; Wei, D. Q.; Zhou, Y. Structure of Microarc Oxidized Coatings Containing Si, Ca and Na on Titanium and Deposition of

Cefazolin Sodium/Chitosan Composite Film. *Surf. Coat. Technol.* **2011**, *205*, 3798−3804.
(16) Song, W. H.; Jun, Y. K.; Han, Y.; Hong, S. H. Biomimetic Apatite Coatings on Micro-Arc Oxidized Titania. *Biomaterials* **2004**, *25*, 3341−3349.
(17) Ramaswamy, Y.; Wu, C. T.; Zhou, H.; Zreiqat, H. Biological Response of Human Bone Cells to Zinc-Modified Ca−Si-Based Ceramics. *Acta Biomater.* **2008**, *4*, 1487−1497.
(18) Yan, Y. Y.; Sun, J. F.; Han, Y.; Li, D. C.; Cui, K. Microstructure and Bioactivity of Ca, P and Sr Doped TiO_2 Coating Formed on Porous Titanium by Micro-Arc Oxidation. *Surf. Coat. Technol.* **2010**, *205*, 1702−1713.
(19) Wei, D. Q.; Zhou, Y. Preparation, Biomimetic Apatite Induction and Osteoblast Proliferation Test of TiO_2-Based Coatings Containing P with a Graded Structure. *Ceram. Int.* **2009**, *35*, 2343−2350.
(20) Yao, Z. Q.; Ivanisenko, Y.; Diemant, T.; Caron, A.; Chuvilin, A.; Jiang, J. Z.; Valiev, R. Z.; Qi, M.; Fecht, H. J. Synthesis and Properties of Hydroxyapatite-Containing Porous Titania Coating on Ultrafine-Grained Titanium by Micro-Arc Oxidation. *Acta Biomater.* **2010**, *6*, 2816−2825.
(21) Cheng, S.; Wei, D. Q.; Zhou, Y. Mechanical and Corrosion Resistance of Hydrophilic Sphene/Titania Composite Coatings on Titanium and Deposition and Release of Cefazolin Sodium/Chitosan Films. *Appl. Surf. Sci.* **2011**, *257*, 2657−2664.
(22) Wei, D. Q.; Zhou, R.; Cheng, S.; Feng, W.; Li, B. Q.; Wang, Y. M.; Jia, D. C.; Zhou, Y.; Guo, H. F. Microarc Oxidized TiO_2 Based Ceramic Coatings Combined with Cefazolin Sodium/Chitosan Composited Drug Film on Porous Titanium for Biomedical Applications. *Mater. Sci. Eng., C* **2013**, *33*, 4118−4125.
(23) Zhou, R.; Wei, D. Q.; Cheng, S.; Zhou, Y.; Jia, D. C.; Wang, Y. M.; Li, B. Q. The Effect of Titanium Bead Diameter of Porous Titanium on the Formation of Micro-Arc Oxidized TiO_2-Based Coatings Containing Si and Ca. *Ceram. Int.* **2013**, *39*, 5725−5732.
(24) Zhou, R.; Wei, D. Q.; Cheng, S.; Li, B. Q.; Wang, Y. M.; Jia, D. C.; Zhou, Y.; Guo, H. F. The Structure and in vitro Apatite Formation Ability of Porous Titanium Covered Bioactive Microarc Oxidized TiO_2-Based Coatings Containing Si, Na and Ca. *Ceram. Int.* **2014**, *40*, 501−509.
(25) Zhou, R.; Yang, H. Y.; Wei, D. Q.; Cheng, S.; Feng, W.; Li, B. Q.; Wang, Y. M.; Jia, D. C.; Zhou, Y. Osseointegration of Bioactive Microarc Oxidized Amorphous Phase/TiO_2 Nanocrystals Composited Coatings on Titanium after Implantation into Rabbit Tibia. *J. Mater. Sci.: Mater. Med.* **2014**, DOI: 10.1007/s10856-014-5154-z.
(26) Zhang, N.; Molenda, J. A.; Fournelle, J. H.; Murphy, W. L.; Sahai, N. Effects of Pseudowollastonite ($CaSiO_3$) Bioceramic on in vitro Activity of Human Mesenchymal Stem Cells. *Biomaterials* **2010**, *31*, 7653−7665.
(27) Nayab, S. N.; Shinawi, L.; Hobkirk, J.; Tate, T. J.; Jones, F. H.; Olsen, I. Adhesion of Bone Cells to Ion-Implanted Titanium. *J. Mater. Sci.: Mater. Med.* **2003**, *14*, 991−997.
(28) Zhou, R.; Yang, H. Y.; Feng, W.; Wei, D. Q.; Cheng, S.; Li, B. Q.; Wang, Y. M.; Jia, D. C.; Zhou Y. Microstructure and MC3T3-E1 Cells Response of Amorphous Phase/TiO_2 Nanocrystals Composited Coating Prepared by Microarc Oxidation on Titanium *Mater. Sci. Eng., C* **2014**; DOI: 10.1016/j.msec.2014.03.006.
(29) Schouten, C.; Meijer, G. J.; van den Beucken, J. J. J. P.; Spauwen, P. H. M.; Jansen, J. A. The Quantitative Assessment of Peri-Implant Bone Responses Using Histomorphometry and Micro-Computed Tomography. *Biomaterials* **2009**, *30*, 4539−4549.
(30) Anselme, K. Osteoblast Adhesion on Biomaterials. *Biomaterials* **2000**, *21*, 667−681.
(31) Boyan, B. D.; Humert, T. W.; Dean, D. D.; Schwartz, Z. Role of Material Surfaces in Regulating Bone and Cartilage Cell Response. *Biomaterials* **1996**, *17*, 137−146.
(32) Anselme, K.; Bigerelle, M.; Noel, B.; Dufresne, E.; Judas, D.; Iost, A.; Hardouin, P. Qualitative and Quantitative Study of Human Osteoblast Adhesion on Materials with Various Surface Roughnesses. *J. Biomed. Mater. Res.* **2000**, *49*, 155−166.
(33) Kieswetter, K.; Schwartz, Z.; Humrnert, T. W.; Cochran, D. L.; Simpson, J.; Dean, D. D.; Boyan, B. D. Surface Roughness Modulates the Local Production of Growth Factors and Cytokines by Osteoblast-Like MG-63 Cells. *J. Biomed. Mater. Res.* **1996**, *32*, 55−63.
(34) Das, K.; Bose, S.; Bandyopadhyay, A. Surface Modifications and Cell-Materials Interactions with Anodized Ti. *Acta Biomater.* **2007**, *3*, 573−585.
(35) Takebe, J.; Itoh, S.; Okada, J.; Ishibashi, K. Anodic Oxidation and Hydrothermal Treatment of Titanium Results in a Surface That Causes Increased Attachment and Altered Cytoskeletal Morphology of Rat Bone Marrow Stromal Cells in vitro. *J. Biomed. Mater. Res.* **2000**, *51*, 398−407.
(36) Zhang, Y. M.; Bataillon-Linez, P.; Huang, P.; Zhao, Y. M.; Han, Y.; Traisnel, M.; Xu, K. W.; Hildebrand, H. F. Surface Analyses of Micro-Arc Oxidized and Hydrothermally Treated Titanium and Effect on Osteoblast Behavior. *J. Biomed. Mater. Res., Part A* **2004**, *68*, 383−391.
(37) Deligianni, D. D.; Katsala, N. D.; Koutsoukos, P. G.; Missirlis, Y. F. Effect of Surface Roughness of Hydroxyapatite on Human Bone Marrow Cell Adhesion, Proliferation, Differentiation and Detachment Strength. *Biomaterials* **2001**, *22*, 87−96.
(38) Castellani, R.; de Ruijter, A.; Renggli, H.; Jansen, J. Response of Rat Bone Marrow Cells to Differently Roughened Titanium Discs. *Clin. Oral Implan. Res.* **1999**, *10*, 369−378.
(39) Kunzler, T. P.; Drobek, T.; Schuler, M.; Spencer, N. D. Systematic Study of Osteoblast and Fibroblast Response to Roughness by Means of Surface-Morphology Gradients. *Biomaterials* **2007**, *28*, 2175−2182.
(40) Ponader, S.; Vairaktaris, E.; Heinl, P.; Wilmowsky, C. V.; Rottmair, A.; Koerner, C.; Singer, R. F.; Holst, S.; Schlegel, K. A.; Neukarn, F. W.; Nkenke, E. Effects of Topographical Surface Modifications of Electron Beam Melted Ti-6Al-4V Titanium on Human Fetal Osteoblasts. *J. Biomed. Mater. Res., Part A* **2008**, *84*, 1111−1119.
(41) Hatano, K.; Inoue, H.; Kojo, T.; Matsunaga, T.; Tsujisawa, T.; Uchiyama, C.; Uchida, Y. Effect of Surface Roughness on Proliferation and Alkaline Phosphatase Expression of Rat Calvarial Cells Cultured on Polystyrene. *Bone (N. Y., NY, U. S.)* **1999**, *25*, 439−445.
(42) Zhao, G.; Zinger, O.; Schwartz, Z.; Wieland, M.; Landolt, D.; Boyan, B. D. Osteoblast-Like Cells Are Sensitive to Submicron-Scale Surface Structure. *Clin. Oral Implan. Res.* **2006**, *17*, 258−264.
(43) Marinucci, L.; Balloni, S.; Becchetti, E.; Belcastro, S.; Guerra, M.; Calvitti, M.; Lilli, C.; Calvi, E. M.; Locci, P. Controlled Release of Fibroblast Growth Factor 2 Stimulates Bone Healing in an Animal Model of Diabetes Mellitus. *Int. J. Oral Max. Implan.* **2006**, *21*, 719−725.
(44) Lohmann, C. H.; Bonewald, L. F.; Sisk, M. A.; Sylvia, V. L.; Cochran, D. L.; Dean, D. D.; Boyan, B. D.; Schwartz, Z. Maturation State Determines the Response of Osteogenic Cells to Surface Roughness and 1,25-Dihydroxyvitamin D_3. *J. Bone Miner. Res.* **2000**, *15*, 1169−1180.
(45) Anselme, K.; Bigerelle, M. Topography Effects of Pure Titanium Substrates on Human Osteoblast Long-Term Adhesion. *Acta Biomater.* **2005**, *1*, 211−222.